BMC Women's Health

RESEARCH

Open Access

PCOS combined with obesity aggravates the metabolic and immune abnormality in females

Mei-Ling Chen[1†], Shu-Ping Zhang[1,3†], Jie Yang[1†], Peng-Fei Qin[2†], Jia-Qi Liu[1,3†], Ning Su[1,3], Yan-Li Sun[2], Lin Gu[2], Zhi-Xia Yang[5], Jie Chen[2*], Xian-Zhe Gu[4*], Ping Zhou[1*], Dong Zhang[1,3*] and Qian Li[2*]

Abstract

Introduction Polycystic ovary syndrome (PCOS) appears to be closely correlated with obesity; however, no studies have compared the difference between PC-Ob (PCOS plus obesity), obesity-only, and PCOS-only patients at a multi-omics level. In the present study, we aimed to explore this through sEV proteomics and metabolomics on female plasma.

Methods We recruited 79 females based on BMI, AMH, LH, T, P, Fasting insulin, and HOMA-IR; next, we categorized them into four groups: 20 Control (Ctr), 21 PCOS, 19 Obesity (Ob), and 19 PCOS with Obesity (PC-Ob) and collected plasma samples. Next, we randomly sent 10 from each group for quantitative sEV proteomics and untargeted metabolomics on female plasma.

Results There were significant changes in multiple metabolites and proteins between each of three patient (PCOS, Ob, and PC-Ob) groups and Ctr group. Particularly, compared with PCOS or Ob group, PC-Ob group have more DEPs (differentially-expressed proteins) and MLDs (metabolites with level difference), and the proteins are largely involved in immunity and metabolism. Cross-omics associations analysis showed that two immunity and metabolism-related DEPs, A2M and BCHE, changes in high correlation with multiple lipids between the upper four groups.

Discussion Our findings showed that females with both PCOS and obesity have significantly increased abnormalities in immunity and metabolism.

†Mei-Ling Chen, Shu-Ping Zhang, Jie Yang, Peng-Fei Qin and Jia-Qi Liu contributed equally to this work.

*Correspondence:
Jie Chen
ejiechen@163.com
Xian-Zhe Gu
13339282298@163.com
Ping Zhou
zhoup_325@aliyun.com
Dong Zhang
dong.ray.zhang@ahmu.edu.cn
Qian Li
drliqian@njmu.edu.cn

Full list of author information is available at the end of the article

Introduction

Polycystic ovary syndrome (PCOS) is a common endocrine disorder that affects female fertility. Its main features include polycystic ovaries, ovulation disorder, and abnormal androgen levels, which can lead to various symptoms, including menstrual disorders, hirsutism, acne, obesity, and acanthosis nigricans ([1–2]). Patients with PCOS also frequently have other health problems, including metabolic [3–5], immune [6–9], and inflammatory [10–13] disorders.

Obesity is defined as a body mass index (BMI) of > 24 kg/m^2. While obesity is not a disorder itself, excessive fat

Keywords PCOS, Obesity, Metabolic, Immune, females

frequently induces abnormalities in metabolism [14–17], immune response [18], microbiota [19], and endocrine systems [20]. It is also a risk factor for fatty liver disease [21], atherosclerosis [22], inflammatory disorders [23], and tumorigenesis [24]. Patients living with obesity are also more likely to develop PCOS, and weight loss can help recover fertility in patients with PCOS [25–27].

Therefore, important questions are whether there is experimental evidence of an increased risk of obesity in patients with PCOS or animal models and whether individuals or mouse models with obesity are at increased risk of PCOS. In clinical cases, it has been noted that while the prevalence of PCOS is lower in those with BMIs of 30–34 kg/m^2, the overall incidence of PCOS increases with increasing BMI [28].

Moreover, the mean BMI is significantly higher among women with PCOS than among women without PCOS, suggesting mutual promotion between PCOS and obesity in clinical settings [28]. In a mouse model of PCOS, inflammatory markers were higher in obese mice than in non-obese mice [29]. Additionally, mice with PCOS were more susceptible to obesity than those without PCOS [30]. These findings suggest that in animal models, PCOS development and progression are mutually reinforcing with obesity.

Consequently, while a causal relationship between obesity and PCOS has not been fully established, they appear closely associated. Sequencing analysis of 16 samples of ovarian granulosa cells revealed that the co-occurrence of obesity and PCOS significantly exacerbated immune dysfunction in patients [31]. Specifically, patients with PCOS and obesity had a markedly higher number of differentially expressed immune-related genes (n = 16) than those with PCOS (n = 9) or obesity (n = 2) alone. This finding suggests that the coexistence of obesity and PCOS may intensify immune system abnormalities by upregulating genes involved in immune regulation [28]. Moreover, obesity not only exacerbates common phenotypes in PCOS [28], such as impaired glucose tolerance and dyslipidemia, but also reduces the effectiveness of infertility treatments. Research indicates that being overweight or obese can disrupt normal metabolic processes in patients with PCOS, adversely affecting reproductive health and therapeutic interventions [28]. These findings underscore the importance of considering patient weight status in managing PCOS to optimize clinical outcomes and enhance overall patient well-being.

However, no studies have yet compared those with PCOS and obesity, obesity alone, and PCOS alone at a multi-omics level. In the present study, we use quantitative proteomics and metabolomics on female plasma to demonstrate for the first time that females with PCOS and obesity exhibit various distinct characteristics from those with either obesity or PCOS.

Materials and methods

Human sample collection and grouping

This study recruited 79 females at the Department of Gynecology, Nanjing Women and Children's Healthcare Hospital, to compare patients with obesity and PCOS (n = 19; PC-Ob group), obesity only (n = 19; Ob group), and PCOS only (n = 21; PCOS group), as well as healthy controls (n = 20; Ctr group). The groupings were verified through BMI; levels of anti-Müllerian hormone (AMH), luteinizing hormone (LH), testosterone (T), progesterone (P), and fasting insulin; and homeostatic model assessment of insulin resistance (HOMA-IR; Table 1).

Participants were placed into three categories based on BMI (kg/m^2): normal (18.5–25 kg/m^2), overweight (25–30 kg/m^2), and obese (≥ 30 kg/m^2) [32]. PCOS was diagnosed according to the International Evidence-Based Guideline for the Assessment and Management of Polycystic Ovary Syndrome 2018, which requires the presence of any two of hyperandrogenism, ovulatory dysfunction, and polycystic ovarian morphology [33]. The inclusion criteria for patients were being 18–35 years old, not receiving hormonal therapy previously or having discontinued such therapy at least three months ago, and having no significant concomitant medical or surgical conditions. Only a blood sample was collected from each patient, and no intervention was given. The number of enrolled patients was determined based on previous studies [14–18].

For quantitative proteomic and metabolomic analyses, samples from ten patients in each group were randomly selected using an online random number generator (https://www.jyshare.com/front-end/6680/).

SEV isolation

SEV extraction was conducted as reported [34]. Briefly, 1 mL of plasma was collected from 79 healthy volunteers, kept on ice, and processed within 24 h. Their age, gender, and health status were recorded. Individuals with known diseases or taking medication were excluded. The samples were centrifuged at 4,600 rpm and room temperature for 30 min, mixed with VEX reagent (Cat no. R603, Vazyme, Nanjing, China), incubated at 2–8 °C for 30 min, and then recentrifuged at 9,600 rpm and room temperature for 5 min. Then, the sEV concentrate was resuspended in phosphate-buffered saline (PBS), aliquoted (100 μL), and stored at – 80 °C for up to six months. Before use, samples were thawed on ice and then

Table 1 Human sample collection and grouping

Parameters	Ctr	Ob	PCOS	PC-Ob	*p*-value
Sample size	20	19	21	19	
BMI(Kg/m^2)	21.4 ± 2.0	32.6 ± 2.9	22.4 ± 1.7	33.5 ± 3.0	< 0.0001
Age(years)	28.0 ± 4.8	26.3 ± 5.7	24.5 ± 4.8	25.6 ± 5.7	ns
AMH(ng/mL)	6.6 ± 4.8	3.4 ± 1.4	10.1 ± 5.7	9.6 ± 5.5	0.0018
FSH(mIU/mL)	6.1 ± 2.4	6.2 ± 3.0	5.2 ± 1.9	5.6 ± 1.3	ns
LH(mIU/mL)	8.3 ± 4.7	6.8 ± 5.5	14.9 ± 7.7	11.9 ± 6.9	0.0036
T(ng/mL)	0.4 ± 0.2	0.5 ± 0.2	0.8 ± 0.4	0.8 ± 0.3	0.0006
P(ng/mL)	4.3 ± 5.6	1.6 ± 2.7	1.1 ± 2.0	0.4 ± 0.2	0.0082
E2(pg/mL)	62.6 ± 45.7	63.0 ± 69.9	81.5 ± 47.4	61.5 ± 40.5	ns
PRL(ng/mL)	21.3 ± 13.4	19.0 ± 15.2	28.6 ± 42.8	14.3 ± 5.5	ns
Fasting insulin(pmol/L)	7.7 ± 3.3	13.8 ± 5.3	7.5 ± 2.5	18.1 ± 10.9	0.0027
Fasting glucose(mmol/L)	5.1 ± 0.2	5.4 ± 0.9	5.7 ± 1.3	5.1 ± 0.5	ns
HOMA-IR	1.0 ± 0.9	3.1 ± 1.3	1.9 ± 0.9	3.9 ± 2.7	0.0073

Four groups were collected and categorized: 20 control females (Ctr); 19 females with obesity only (Ob); 21 females with PCOS only (PCOS), and 19 females with PCOS plus obesity (PC-Ob). Grouping was verified through BMI, AMH, LH, T, P, Fasting insulin, and HOMA-IR

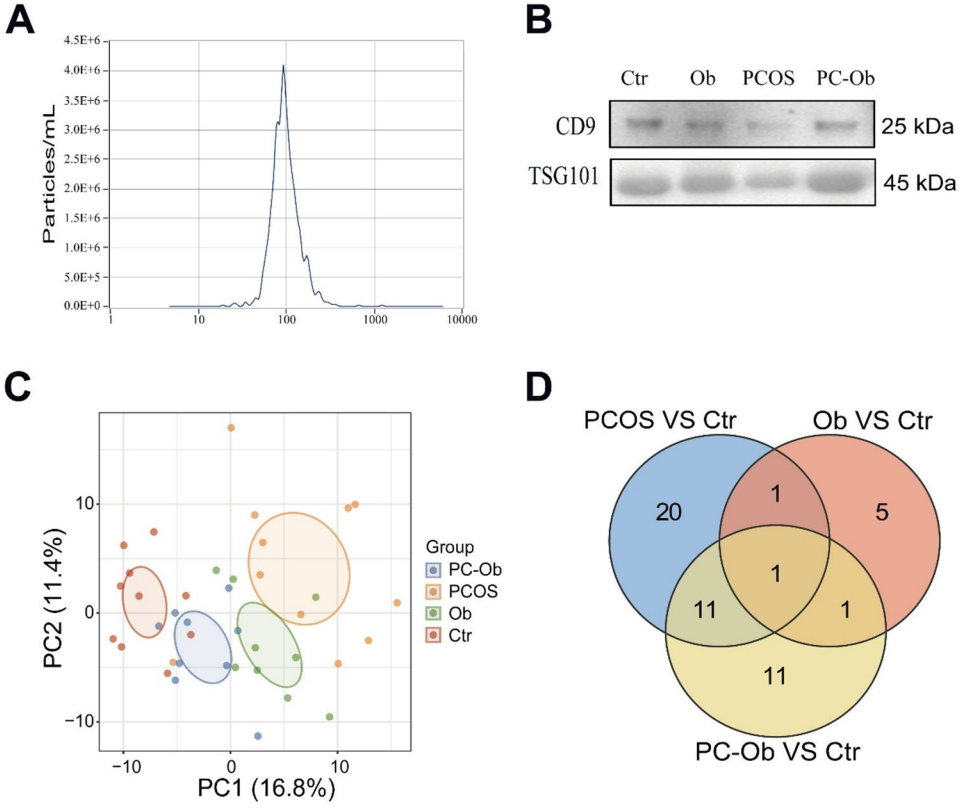

Fig. 1 Characterization of plasma sEV. **A** Particle analysis showed that the size of the purified sEVs peaked at 100 nm. **B** Western blot showed that purified sEVs expressed classical sEV markers CD9 and TSG101. **C** Principal component (PC) analysis of plasma sEV proteomics showed clear separation of the protein expression profiles of Ctr, PCOS, Ob, and PC-Ob groups. **D** Pie chart analysis of differentially-expressed proteins (DEPs; fold change > 2.0 or < 0.5, $p < 0.05$) between PCOS and Ctr, Ob and Ctr, PC-Ob and Ctr showed that the DEPs were largely distinct from each other, albeit with partial overlap

centrifuged at 12,000 rpm and 4 °C for 10 min to remove precipitates. The quality of the sEV was verified by particle analysis (Fig. 1A), western blot of sEV marker proteins (Fig. 1B), and analysis of the correlation between DEPs (in Fig. 2A and F) and sEV or vesicle (Suppl. Figure 1A and 1B).

Nanoparticle tracking analysis

The size distribution of the isolated sEVs was determined via nanoparticle tracking analysis using a Zeta-View instrument (Particle Metrix). The samples were diluted with PBS before analysis. Both the sizes and

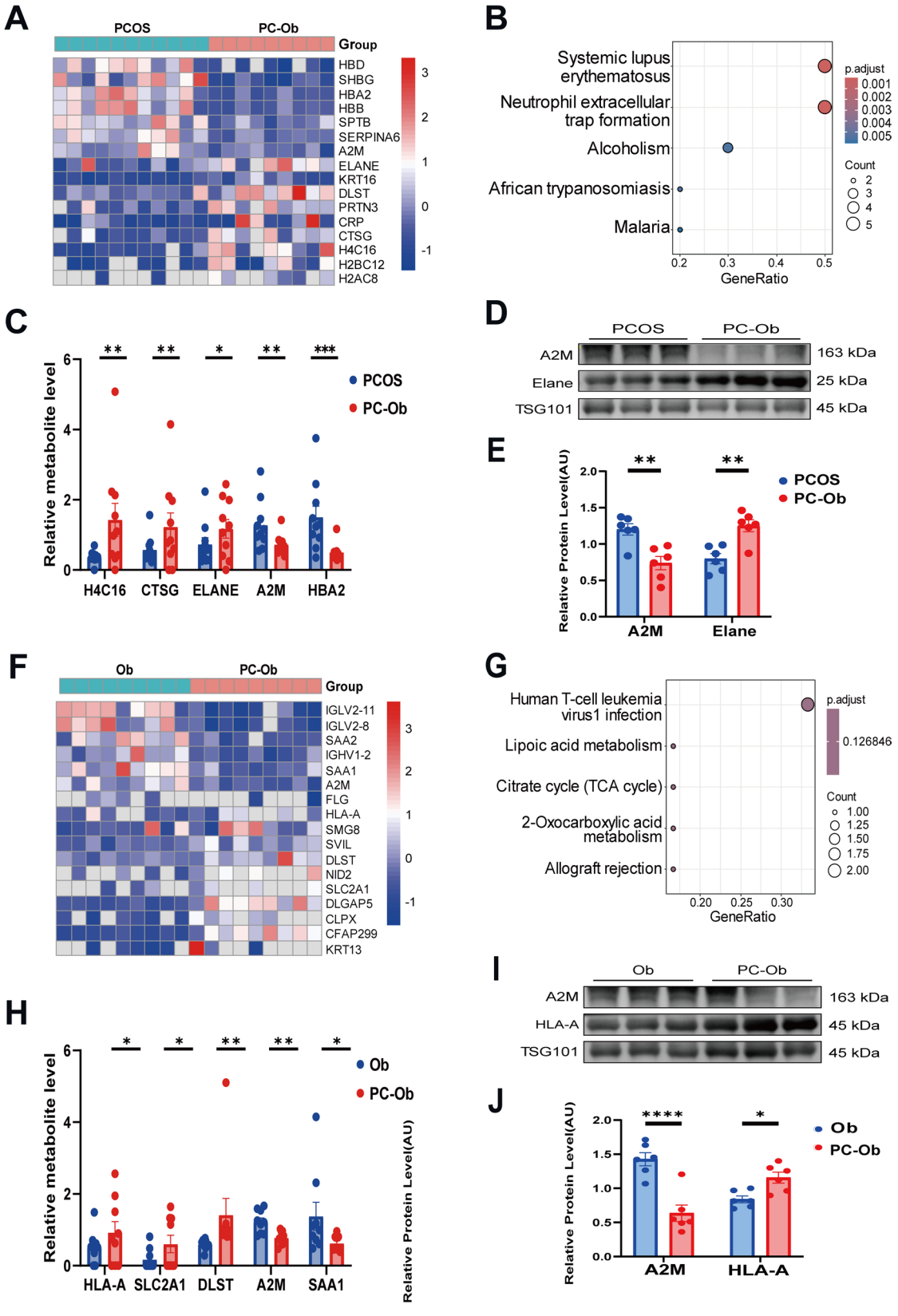

Fig. 2 (See legend on next page.)

(See figure on previous page.)

Fig. 2 Quantitative proteomics of plasma sEVs showed that PC-Ob subjects are distinct from those with PCOS or Obesity alone. **A** and **B** Heat maps showed that there are 9 upregulated and 7 downregulated DEPs between PCOS-Ob and PCOS (fold change > 2.0 or < 0.5, $p < 0.05$); KEGG analysis showed that these DEPs were involved in systemic lupus erythematosus, neutrophil extracellular trap formation, alcoholism, african trypanosomiasis, and malaria processes. **C** Representative graphs from **A**. **D** and **E** Blot verification of representative DEPs (A2M, ELANE) in **C**. **F** and **G** There were 10 upregulated and 7 downregulated DEPs between PCOS-Ob and Ob (fold change > 2.0 or < 0.5, $p < 0.05$); KEGG analysis showed that these DEPs were involved in Human T-cell leukemia virus1 infection, lipoic acid metabolism, citrate cycle (TCA cycle), 2-Oxocarboxylic acid metabolism, and allograft rejection processes. **H** Representative graphs from **F**. **I** and **J** Blot verification of representative DEPs in **H**. *, $p < 0.05$; **, $P < 0.01$; ***, $P < 0.001$

concentrations of the nanoparticles were assessed using ZetaView software.

SEV proteomics

For sEV protein extraction, four volumes of lysis buffer (8 M urea and 1% protease inhibitor cocktail) were added, and the mixture was sonicated for 3 min on ice using a high-intensity ultrasonic processor (Scientz). Next, the lysate was centrifuged at 12,000 g and 4 °C for 10 min to remove debris, and the supernatant was collected. Then, the protein concentration was determined using a bicinchoninic acid assay according to the manufacturer's instructions.

Next, the protein solution was reduced with 5 mM dithiothreitol at 56 °C for 30 min, followed by alkylation with 11 mM iodoacetamide at room temperature for 15 min in the dark. Then, the sample was diluted with 200 mM triethylammonium bicarbonate to reduce the urea concentration below 2 M. Next, it was digested with trypsin at a 1:50 trypsin-to-protein mass ratio overnight and at a 1:100 ratio for an additional four hours.

Then, the peptides were desalted using a Strata X SPE column. The tryptic peptides were then dissolved in solvent A (0.1% formic acid and 2% acetonitrile in water) and loaded onto a homemade reversed-phase analytical column (25 cm length, 100 μm i.d.) for liquid chromatography-mass spectrometry analysis using an EASY-nLC 1200 UPLC system coupled to an Orbitrap Exploris 480 mass spectrometer. Finally, the peptides were separated using a gradient of solvent A and solvent B (0.1% formic acid and 90% acetonitrile in water) and analyzed using a high-resolution mass spectrometry scan.

Next, the data-independent acquisition (DIA) data were processed using the DIA-NN search engine (v.1.8) and searched against the Homo_sapiens_9606_SP_20230103.fasta database. Trypsin/P was specified as the cleavage enzyme, and one missed cleavage was allowed. N-terminal methionine excision and carbamidomethylation on cysteine were set as fixed modifications. The false discovery rate was maintained below 1%. Gene ontology analysis was conducted using eggNOG-mapper, classifying proteins into cellular components, molecular functions, and biological processes. Structural domains were annotated using the Pfam database. Kyoto Encyclopedia of Genes and Genomes (KEGG) pathways were identified through BLAST comparison. Subcellular localization was predicted using WolF PSORT and PSORTb software for eukaryotic and prokaryotic proteins, respectively. Functional enrichment and clustering analyses were conducted using Fisher's exact test and hierarchical clustering, visualized via heat maps and the STRING database for protein-protein interaction networks.

SEVs western blot

Briefly, sEVs were resuspended in protein sample buffer (Yeason, Cat No 20315ES, Shanghai, China) at 0.1 mg/mL of protein conc., boiled for 5 min and stored at -20 °C. 20 μL ready-to-use sample each well was separated in 10% polyacrylamide gels and transferred onto a PVDF membrane using a fast transfer system (GenScript, Nanjing, China). The PVDF membrane was blocked with 5% non-fat milk diluted with TBST (TBS containing 0.1% Tween-20) for 1 h at room temperature and then incubated with primary antibody (diluted with 5% nonfat milk) overnight at 4 °C. The PVDF membrane was washed three times, incubated with HRP-conjugated secondary antibody (Beyotime, Cat No A0208, Beijing, China, 1:10000 diluted with 5% nonfat milk) for 1 h at room temperature, washed three times, and finally developed by an SuperFemto ECL Chemiluminescence Kit (Vazyme, Cat No E423-02, Nanjing, China) and detected by a digital chemiluminescence imaging system (Tanon, Nanjing, China).

Primary antibody: Mouse anti-CD9 Monoclonal antibody (Proteintech, Cat No 60232-1-Ig, Chicago, USA, 1:5000); Rabbit anti-TSG101 Polyclonal Antibody (Beyotime, Cat No AF8259, Shanghai, China, 1:1000). We used both CD9 and TSG101 for sEV validation (Fig. 1B), since we found that the proper exposure time for these two antibodies were significantly different, to avoid their mutual interference, we detected them on separate PVDF membrane.

Plasma untargeted metabolomics

Briefly, 200 mL of plasma per sample was sent to a professional company (Wuhan Metware Biotechnology, Wuhan, Hubei, China) for full spectrum metabolomic analysis, which covers all kinds of metabolites, to initially screen for metabolites differing significantly between the Ctr, PCOS, Ob, and PC-Ob groups. The analytical platform was Waters Acquity I-Class PLUS ultra-high-performance liquid chromatographer coupled with a Waters Xevo G2-XS QTOF high-resolution mass spectrometer. The samples were analyzed according to the

specified parameters. The raw data obtained using the MassLynx V4.2 software were processed with Progenesis QI for peak extraction, alignment, and further processing. Metabolites were identified using the Progenesis QI software with the online METLIN database, publicly accessible databases, and a custom-built BMKGENE database. Theoretical fragments were identified, maintaining a mass deviation threshold within 100 ppm for parent ions and 50 ppm for fragment ions.

Statistical analyses

The data are presented as the mean ± standard error of the mean (SEM) and were compared between two groups using Student's *t*-test in Excel (Microsoft, Redmond, WA, USA) and multiple groups using the Kruskal–Wallis one-way nonparametric analysis of variance in Prism (GraphPad Software, San Diego, CA, USA). A $p < 0.05$ was considered statistically significant. The correlation analysis between the proteome and the metabolome was conducted using the Spearman correlation coefficient. All statistical analyses were performed using the R 4.2 software (with the cor.test function, method = "spearman").

Results

Human sample collection and grouping

We first confirmed the experimental groupings using multiple indices (Table 1). AMH levels were notably higher in the PCOS and PC-Ob groups than in the Ob and Ctr groups, suggesting potential differences in ovarian reserve across groups. Regarding the metabolic indicators, fasting insulin levels differed significantly among groups ($p = 0.0027$), while fasting glucose levels did not (nonsignificant [ns]). The HOMA-IR, calculated from fasting glucose and insulin levels, also differed significantly among groups ($p = 0.0073$). Specifically, the HOMA-IR values in the Ob (3.1 ± 1.3) and PC-Ob (3.9 ± 2.7) groups were both above the commonly recognized threshold of 2.5 for insulin resistance, whereas those in the Ctr (1.0 ± 0.9) and PCOS (1.9 ± 0.9) groups were below this threshold. These findings not only confirmed significant differences in insulin sensitivity across groups but also highlighted important distinctions in metabolic status among groups. Based on these data, our groupings were appropriate.

Quantitative proteomics of plasma sEVs showed that the PC-Ob group was distinct from the PCOS and Ob groups

We isolated plasma sEVs for quantitative proteomics to avoid interference from high-abundance proteins (e.g., albumin and immunoglobulin) within the plasma and to more efficiently enrich functional proteins. Particle analysis showed that the sEVs had a peak size of 100 nm (Fig. 1A) and expressed the classical sEV markers CD9 molecule (CD9) and tumor susceptibility 101 (TSG101; Fig. 1B), indicating the successful isolation of plasma sEVs.

Results showed that there are plenty of differentially-expressed proteins (DEPs) between Ctr and each of the three patient groups (Supplementary dataset 1). Principal component (PC) analysis of the plasma sEV proteomic data clearly separated the protein expression profiles of the Ctr, PCOS, Ob, and PC-Ob groups (Fig. 1C). Venn diagram analysis of DEPs (fold change > 2.0 or < 0.5, $p < 0.05$) between the PCOS and Ctr, Ob and Ctr, and PC-Ob and Ctr groups showed that they were largely distinct, albeit with some overlap (Fig. 1D, suppl. Figure 2 A-C). These results suggest that the PC-Ob group was distinct from the PCOS and Ob groups.

Next, we further analyzed the DEPs between PC-Ob and PCOS or PC-Ob and Ob groups. Heat maps showed 9 upregulated and 7 downregulated proteins between the PCOS-Ob and PCOS groups at fold change > 2 or < 0.5. KEGG analysis showed that these DEPs were involved in systemic lupus erythematosus, neutrophil extracellular trap formation, alcoholism, African trypanosomiasis, and malaria processes (Fig. 2A-C). We have verified two representative DEPs, A2M and ELANE (Fig. 2D and E).

Similarly, heat maps showed 10 upregulated and 7 downregulated proteins between the PCOS-Ob and Ob groups. KEGG analysis showed that these DEPs were involved in Human T-cell leukemia virus1 infection, lipoic acid metabolism, citrate cycle (TCA cycle), 2-Oxocarboxylic acid metabolism, and allograft rejection processes (Fig. 2F-H). We have also verified two representative DEPs, A2M and HLA-A (Fig. 2I and J). CoreMine analysis further showed the clear involvement of these DEPs in immunity and metabolism from multiple perspectives and their mutual interaction (Between PCOS-Ob and PCOS, suppl. Figure 3 A and 3B; between PCOS-Ob and Ob, suppl. Figure 4 A and 4B).

Quantitative metabolomics of plasma showed that the PC-Ob group was distinct from the PCOS and Ob groups

PCOS and obesity are usually accompanied by abnormal metabolism [3–5, 14]. Therefore, we examined participants' metabolic status through quantitative metabolomics. First, we analyze the metabolomics in the positive ion mode. PC analysis of the plasma metabolomics showed that metabolite profiles differed somewhat between the Ctr, PCOS, Ob, and PC-Ob groups, albeit with substantial overlap (Fig. 3A). Venn diagram analysis of differential metabolites (fold change > 1.6 or < 0.625, $p < 0.05$) between the PCOS and Ctr, Ob and Ctr, and PC-Ob and Ctr groups showed largely distinct levels for many metabolites, albeit with some overlap (Fig. 3B; supplementary dataset 2; suppl. Figure 5 A-C). These results suggest that the PC-Ob group was distinct from the PCOS and Ob groups.

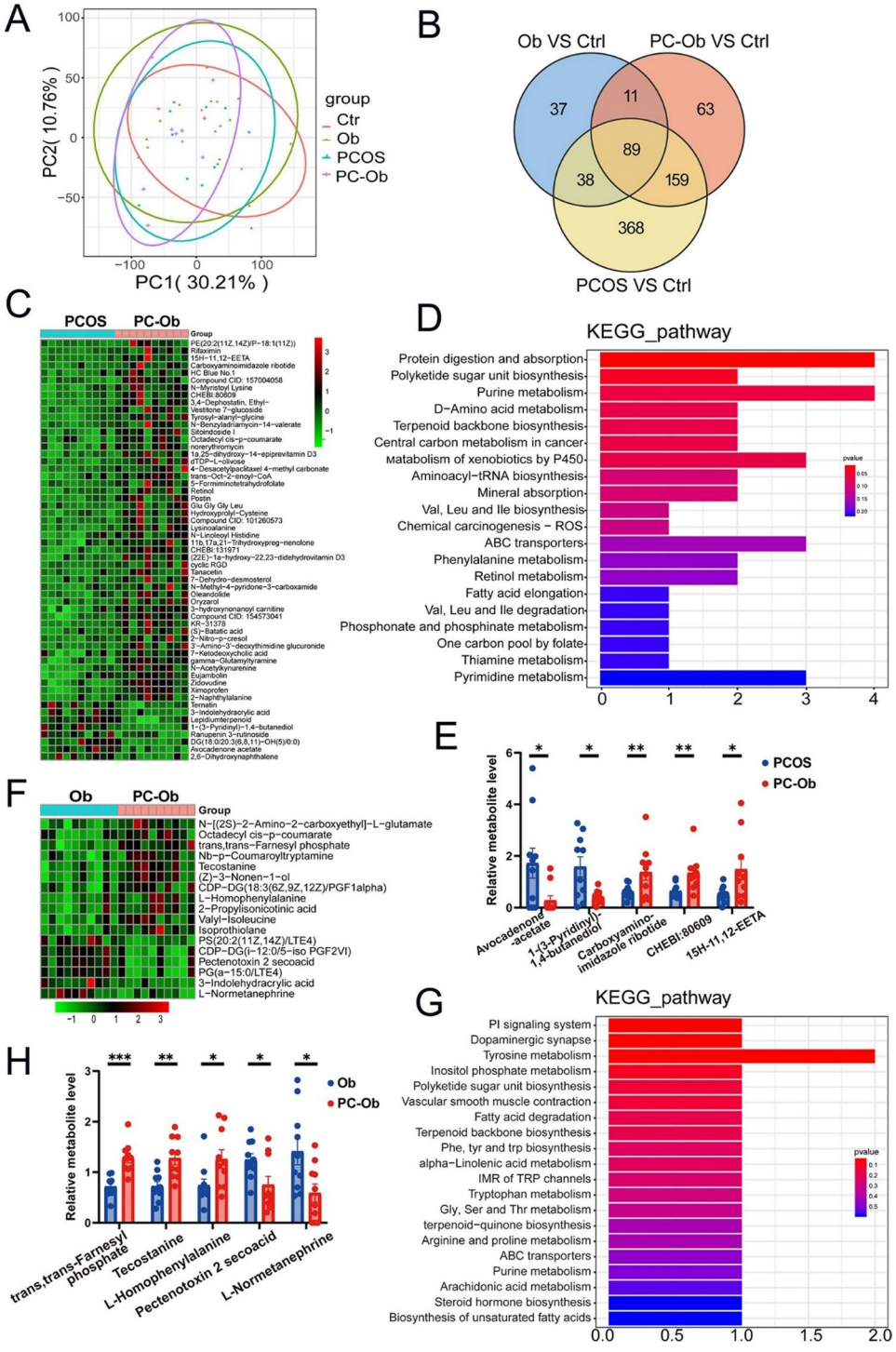

Fig. 3 Positive-ion metabolites of PC-Ob patients are distinct from those with PCOS or Obesity alone. **A** PC analysis of plasma metabolomics showed that the positive-ion metabolite profiles of Ctr, PCOS, Ob, and PC-Ob groups were somewhat distinct from each other, but with substantial overlap. **B** Pie chart analysis of different positive-ion metabolites (fold change > 1.6 or < 0.625, $p < 0.05$) between PCOS and Ctr, Ob and Ctr, PC-Ob and Ctr showed that the levels of many positive-ion metabolites were largely distinct from each other, with some overlap. **C** and **D** Heat mapping showed that there are 49 upregulated and 8 downregulated positive-ion metabolites between PC-Ob and PCOS (**C**); KEGG analysis showed that these metabolites were involved in the biosynthesis and metabolism of many important fundamental nutritional small molecules (**D**). **E** Representative graphs from **C**. **F** and **G**. Heat mapping showed that there were 11 upregulated and 6 downregulated positive-ion metabolites between PC-Ob and Ob (**F**); KEGG analysis showed that these metabolites were involved in the biosynthesis and metabolism of many important fundamental nutritional small molecules (**G**)**. H** Representative graphs from **F**. *, $p < 0.05$; **, $P < 0.01$; ***, $P < 0.001$

Next, we further analyzed the differential metabolites between the PC-Ob and PCOS or PC-Ob and Ob groups. Heat maps showed 49 upregulated and 8 downregulated metabolites between the PCOS-Ob and PCOS groups. KEGG analysis showed that these metabolites were involved in the biosynthesis and metabolism of many important fundamental nutritional small molecules (Fig. 3C-E). Similarly, the heat maps showed 11 upregulated and 6 downregulated metabolites between the PCOS-Ob and Ob groups. KEGG analysis showed them to be involved in the biosynthesis and metabolism of many important fundamental nutritional small molecules (Fig. 3F-H). The metabolites and related KEGG pathways differing between the PCOS-Ob and PCOS groups largely differed from those differing between the PCOS-Ob and Ob groups.

Then, we analyzed the metabolomics in the negative ion mode. Similarly, an analysis of plasma metabolomics showed that metabolite profiles differed somewhat between the Ctr, PCOS, Ob, and PC-Ob groups, albeit with large overlap (Fig. 4A). Venn diagram analysis of the differential metabolites (fold change > 1.6 or < 0.625, $p < 0.05$) between the PCOS and Ctr, Ob and Ctr, and PC-Ob and Ctr groups showed that the levels of many metabolites were largely distinct, albeit with some overlap (Fig. 4B; supplementary dataset 2; suppl. Figure 5D-F). This observation suggests that the PC-Ob group was distinct from the PCOS and Ob groups.

Next, we further analyzed the differential metabolites between the PC-Ob and PCOS or PC-Ob and Ob groups. Heat maps showed 55 upregulated and 18 downregulated metabolites between the PCOS-Ob and PCOS groups. KEGG analysis showed that these metabolites were involved in the biosynthesis and metabolism of many important fundamental nutritional small molecules (Fig. 4C-E). Similarly, the heat maps showed 22 upregulated and 3 downregulated metabolites between the PCOS-Ob and Ob groups. KEGG analysis showed them to be involved in the biosynthesis and metabolism of many important fundamental nutritional small molecules (Fig. 4F-H). The metabolites and related KEGG pathways differing between the PCOS-Ob and PCOS groups largely differed from those differing between the PCOS-Ob and Ob groups.

Last, we also included age as covariate for the upper representative DEPs and MLDs (Figs. 2C and H, 3E and H and 4E and H) and found that the P values for most of these DEPs or MLDs were still below 0.05 (Supplementary dataset 3), indicating that these DEPs or MLDs are stable and reliable markers for the differences between PC-Ob and Ob or between PC-Ob and PCOS.

Cross-omics associations analysis showed the crosstalk between DEPs and lipid metabolism

Both omics datasets share the identical 2 × 2 factorial design (obesity × PCOS), which allows us to explore cross-omics associations at the group level. Specifically, we calculated the mean abundance of each protein and each metabolite within each of the four experimental groups (Ctrl, PCOS, Ob, PC-Ob). We then performed Spearman correlation analysis on these four-point group-mean vectors. This "group-mean profile correlation" reveals whether a protein and a metabolite show coordinated up-or down-regulation across the four conditions, even without individual matching.

We focused on two immune-related DEPs (A2M and BCHE) and all identified lipid metabolites (Supplementary dataset 4). The resulting heatmap (Fig. 5A and 5B) highlights several lipids with $|\rho| > 0.8$ relative to A2M or BCHE, suggesting strong group-level co-variation. For instance, TG(16:0/18:1/18:1) showed a positive correlation with A2M ($\rho = 0.95$), while LPC(18:0) was negatively correlated with BCHE (ρ =-0.90). These findings support a crosstalk between the DEP and lipid metabolic pathways in the context of PCOS complicated by obesity.

Discussion

Our study demonstrated for the first time that women with PCOS and obesity exhibit more severe abnormalities than those with PCOS or obesity alone through systematic plasma sEV quantitative proteomic and plasma metabolomic analyses. Previous studies have demonstrated that among patients with PCOS, those who are obese exhibit a denser gene-disease network than those who are lean in aspects such as insulin synthesis, steroidogenesis, hormonal and metabolic signaling, gonadotropin secretion, cellular structure, and signaling [35]. This observation indicates that obesity and PCOS jointly and broadly impact immune and metabolic functions.

Firstly, our proteomics analysis showed that many DEPs between the PC-Ob and PCOS or PC-Ob and Ob groups are involved in immunity. For example, alpha-2-macroglobulin (A2M) levels were lower in the PC-Ob group than in the PCOS and Ob groups. A2M uses a bait-and-trap mechanism to inhibit a broad spectrum of proteases, including trypsin, thrombin, and collagenase. It can also inhibit inflammation by blocking the interleukin (IL)-1β/nuclear factor kappa B (NF-κB) pathway [36]. The A2M-glucose regulated protein 78 (GRP78) axis promotes anti-bacterial functions by recruiting and enhancing phagocytosis in echinoderms [37].

A2M-loaded microcapsules also enhanced the innate immune response and human leukocyte functions [38]. Dihydrolipoamide S-succinyltransferase (DLST) levels were higher in the PC-Ob group than in the PCOS and Ob groups. DLST has been characterized as a

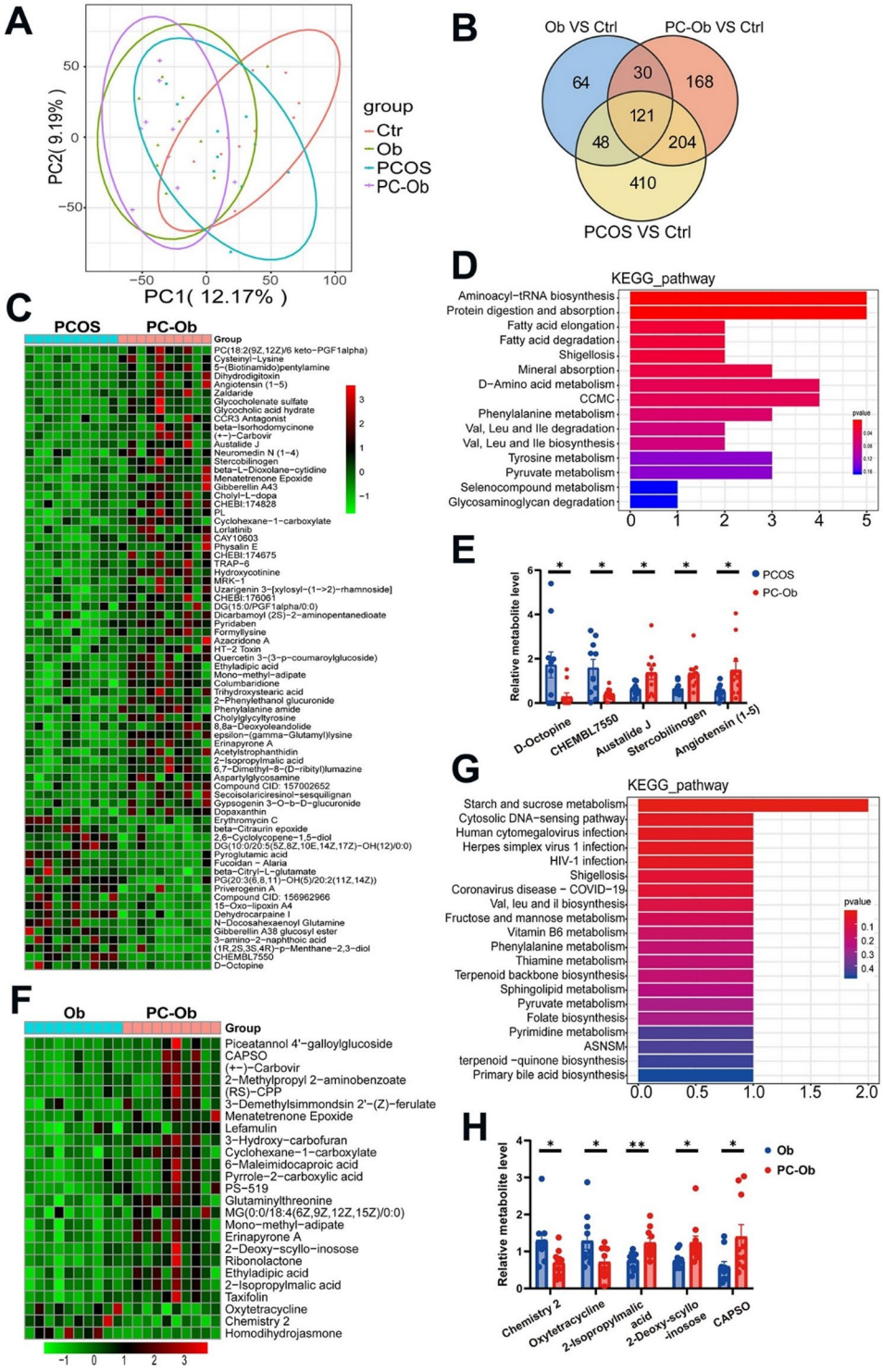

Fig. 4 Negative-ion metabolites of PC-Ob patients are distinct from those with PCOS or Obesity alone. **A** PC analysis of plasma metabolomics showed that the negative-ion metabolite profiles of Ctr, PCOS, Ob, and PC-Ob groups were somewhat distinct from each other, but with large overlap. **B** Pie chart analysis of different negative-ion metabolites (fold change > 1.6 or < 0.625, $p < 0.05$) between PCOS and Ctr, Ob and Ctr, PC-Ob and Ctr showed that the levels of many metabolites are largely distinct from each other, with partial overlap. **C** and **D** Heat maps showed that there were 55 upregulated and 18 downregulated negative-ion metabolites between PCOS-Ob and PCOS (**C**); KEGG analysis showed that these metabolites are involved in the biosynthesis and metabolism of many important fundamental nutritional small molecules (**D**). **E** Representative graphs from **C**. **F** and **G**. Heat maps showed that there were 22 upregulated and 3 downregulated negative-ion metabolites between PCOS-Ob and Ob (**F**), KEGG analysis showed that these metabolites are involved in the biosynthesis and metabolism of many important fundamental nutritional small molecules (**G**). **H** Representative graphs from F. *, $p < 0.05$; **, $P < 0.01$

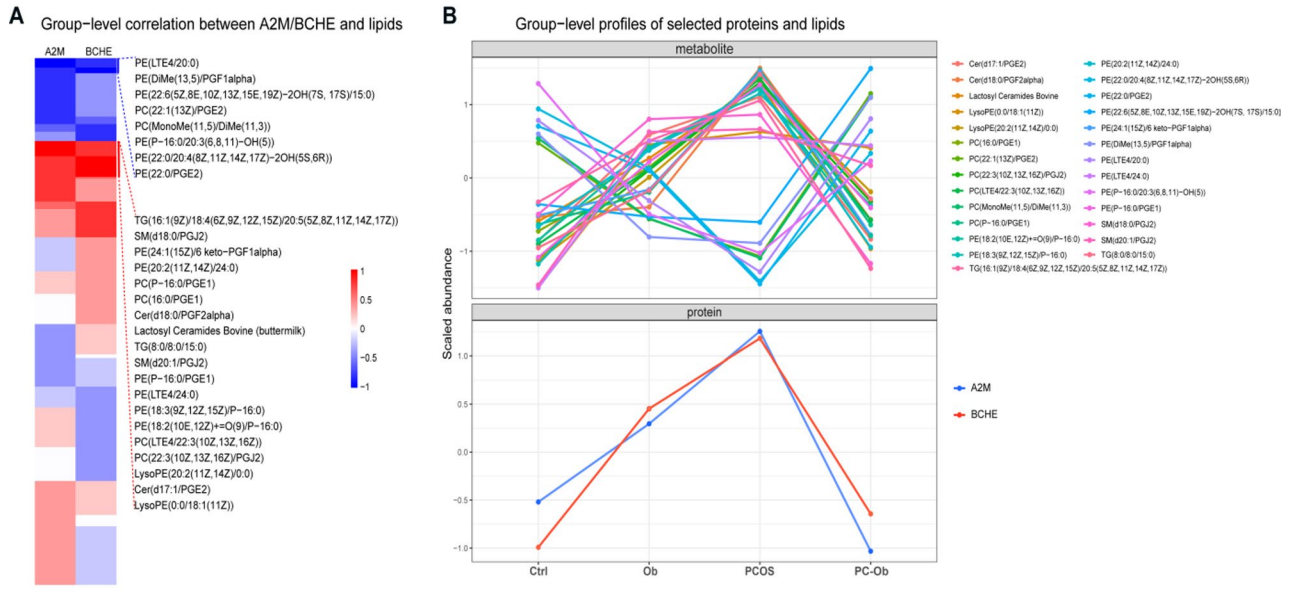

Fig. 5 DEP-lipid correlation analysis between different groups. **A** Group-level correlation between A2M/BCHE and lipid metabolites. Rows represent lipid metabolites (identified by class keywords: TG, PC, PE, SM, Cer, LPC, LPE). Columns represent the two proteins of interest (A2M and BCHE). Color scale indicates Spearman's rank correlation coefficient (ρ) calculated between the four-group mean abundance vectors (Ctrl, PCOS, Ob, PC-Ob) of each lipid and each protein. Blue, negative correlation; red, positive correlation; white, near-zero correlation. This analysis captures coordinated changes at the group level due to non-overlapping sample sets between proteomics and metabolomics. **B** Group-level expression profiles of selected proteins and their strongly correlated lipids. Data are shown as scaled mean abundance (z-score) across (Ctrl, PCOS, Ob, PC-Ob) for each feature. Upper panel: proteins (A2M, BCHE); lower panel: top-ranked lipids (|ρ| > 0.8 with either protein). Lines connect group means to visualize consistent increasing/decreasing trends. Scaling allows comparison of direction and relative change between different molecular types

cuproptosis and immune cell infiltration-related protein and is implicated in periodontitis [39], autism [40], and rheumatoid arthritis [41]. Besides, Cathepsin G (CTSG) showed significant increase in PC-Ob compared with PCOS but not with Ob; CTSG is found in neutrophils and can enter cells via the RAGE receptor, where it degrades the 14-3-3 protein, releases BAX, and ultimately induces apoptosis [42]. Serum amyloid A1 (SAA1) showed significant decrease in PC-Ob compared with Ob but not with PCOS; SAA1 as a major component of acute-phase proteins, SAA1 directly binds LPS to promote LPS uptake by macrophages and reduce inflammation. Inhibiting SAA1-LPS interaction aggravated LPS-induced inflammation [43]. These findings suggest that patients with PCOS and obesity have greater immune abnormalities than those with PCOS or obesity alone.

Secondly, our proteomics analysis showed that many DEPs between PC-Ob and PCOS or PC-Ob and Ob are involved in metabolic processes. For example, butyrylcholinesterase (BCHE) was decreased in the PC-Ob group compared with the PCOS and Ob groups. BCHE catalyzes ghrelin hydrolysis, with BCHE KO shown to increase plasma ghrelin levels and result in increased levels of white fat [44]. BCHE also hydrolyzes and inactivates several anesthetic drugs such as cocaine, heroin, esmolol, local ester anesthetics, and neuromuscular blocking drugs. Inhibition of BCHE with solanaceous glycoalkaloids (SGAs) decreased anesthetic drug metabolism and mivacurium hydrolysis [45]. Nonsense-mediated mRNA decay factor (SMG8) was increased in the PC-Ob group compared with the PCOS and Ob groups. SMG8 is involved in nuclear-transcribed mRNA catabolic processes, nonsense-mediated decay, and regulation of protein kinase activity [46, 47]. In addition, SERPINA6 showed significant decrease in PC-Ob compared with PCOS but not with Ob; SERPINA6 encodes corticosteroid-binding globulin (CBG), which is produced by the liver and regulates the plasma distribution and action of glucocorticoids [48]. Protein SLC2A1 showed significant increase in PC-Ob compared with Ob but not with PCOS; SLC2A1 encodes GLUT1 (glucose transporter 1), a uniporter that transports glucose into mammalian cells [49]. These findings suggest that patients with PCOS and obesity have greater metabolic abnormalities than those with PCOS or obesity alone.

In addition to the proteins highlighted above, various immune- or metabolism-related proteins were upregulated or downregulated in the PC-Ob group compared

to the PCOS or Ob groups, suggesting that the greater immune and metabolic abnormalities in patients with PCOS and obesity could have further significant and extensive impacts.

Our metabolomics analysis showed that in either the positive or negative ion mode, many metabolites that differ between the PC-Ob and PCOS or PC-Ob and Ob groups are involved in the biosynthesis, elongation, degradation, or metabolism of various important nutrients. Therefore, they further support the hypothesis that patients with PCOS and obesity have greater metabolic abnormalities than those with PCOS or obesity alone.

Finally, cross-omics associations analysis showed the probable crosstalk between DEPs (A2M and BCHE) and lipid metabolism, providing an integrative multi-omics insight for the difference between PC-Ob and PCOS or Ob.

However, due to both the distinction and the overlapping between PC-Ob and PCOS or PC-Ob and Ob, their relationship might be more complicated, it's might be hard to say that it's obesity in PCOS patients, or PCOS in obesity patients, lead to exacerbated immunometabolism abnormalities, it could be more like a mutual impact between PCOS and Ob, which is a general phenomenon of the chronic disease caused by mixed factors.

In all, we performed omics analyses of molecular changes in patients with obesity, PCOS, and both conditions, and we also did cross-omics associations analysis to show the crosstalk between DEPs and lipid metabolism. This approach revealed distinct molecular profiles, enhancing the understanding of disease mechanisms. Our results offer insights for clinical risk assessment and early detection, aiding accurate diagnosis of immunological and metabolic issues in patients with PCOS and obesity and supporting personalized treatments. Our findings on combined PCOS and obesity provide a basis for new therapies, improving patient health and quality of life.

However, we must admit that our study has limitations. For example, the sample size for each group is small, which might reduce the credibility of some results; the samples are only from one hospital and most samples are limited to adjacent districts; we used precipitation method to extract sEV, which might cause contamination by non-exosomal particles. Further investigations based on multi-center, large-scale samples, and high-standard sEV extraction method (such as ultracentrifugation or size-exclusion chromatography) are required to discover the mechanism behind the differences between PC-Ob and PCOS or obesity.

Abbreviations

sEVs	Small extracellular vesicles
DEPs	Differentially-expressed proteins
MLDs	Metabolites with level difference
PCOS	Polycystic Ovary Syndrome
HMEC	Human Medical Ethics Committee
PCOM	Polycystic ovarian morphology
Ctr	Control
Ob	Obesity
PC-Ob	PCOS with Obesity
NTA	Nanoparticle tracking analysis
FDR	The false discovery rate
GO	Gene Ontology
KEGG	Kyoto Encyclopedia of Genes and Genomes
ANOVA	One-way analysis of variance
PC	Principal component
A2M	Alpha-2-macroglobulin
GRP78	Glucose Regulated Protein 78
DLST	Dihydrolipoamide S-succinyltransferase
BCHE	Butyrylcholinesterase
SGAs	Solanaceous glycoalkaloids
BMI	Body mass index
SMG8	Nonsense mediated mRNA decay factor
HOMA-IR	Homeostasis model assessment-insulin resistance
IGLV2-8	Immunoglobulin light chain variable region 8 family
IGLV2-11	Immunoglobulin light chain variable region 11 family
SERPINA6	Serine (or cysteine) proteinase inhibitor, clade A, member 6
SHBG	Sex hormone-binding globulin
SLC2A1	Glucose transporter type 1

Supplementary Information

The online version contains supplementary material available at https://doi.org/10.1186/s12905-026-04492-1.

Supplementary Material 1: Supplementary figure 1. A. The correlation of DEPs between PC-Ob and PCOS (Fig. 2C) with sEV through Coremine analysis. B. The correlation of DEPs between PC-Ob and Ob (Fig. 2F) with sEV or vesicle through Coremine analysis or Pubmed search.

Supplementary Material 2: Supplementary figure 2. A and B. Heap map (A) and KEGG (B) of DEPs between Ctr, PCOS, Ob, and PC-Ob groups (fold change > 2 or < 0.5, $p < 0.05$). C. Graphs of DEPs in A.

Supplementary Material 3: Supplementary figure 3. A. CoreMine analysis of the involvement of DEPs between PC-Ob and PCOS in immunity and their mutual interaction. B. CoreMine analysis of the involvement of DEPs between PC-Ob and PCOS in metabolism and their mutual interaction.

Supplementary Material 4: Supplementary figure 4. A. CoreMine analysis of the involvement of DEPs between PC-Ob and Ob in immunity and their mutual interaction. B. CoreMine analysis of the involvement of DEPs between PC-Ob and Ob in metabolism and their mutual interaction.

Supplementary Material 5: Supplementary figure 5. A and B. Heap map (A) and KEGG (B) analysis of MLDs between Ctr, PCOS, Ob, and PC-Ob groups (fold change > 1.6 or < 0.625, $p < 0.05$) at positive-ion mode. C. Representative graphs from A. D and E. Heap map (D) and KEGG (E) analysis of MLDs between between Ctr, PCOS, Ob, and PC-Ob groups (fold change > 1.6 or < 0.625, $p < 0.05$) at negative-ion mode. F. Representative graph from D.

Supplementary Material 6: Supplementary dataset 1. Related to Fig. 2 and Supplementary Fig. 1A-C. This file includes 5 sheets. "All_Data" includes all info. of identified DEPs form Ctr, PCOS, Ob, or PC-Ob group. The other 5 sheets include all DEPs between the upper four groups (fold change > 1.5 or < 0.67, $p < 0.05$).

Supplementary Material 7: Supplementary dataset 2. Related to Fig. 3, 4 and supplementary Fig. 1D-I. This file includes 10 sheets. "All_metabolite_profiles" includes all info. of identified MLDs form Ctr, PCOS, Ob, or PC-Ob group. The other 10 sheets include all MLDs between the upper four groups at negative ion mode or positive ion mode (fold change > 1.5 or < 0.67, $p < 0.05$).

Supplementary Material 8: Supplementary dataset 3. Related to Fig. 2C and 2H, Fig. 3E and 3H, Fig. 4E and 4H. Linear regression analysis of DEPs and MLDs between PC-Ob and PCOS or between PC-Ob and Ob when age was used as covariate.

Supplementary Material 9: Supplementary dataset 4. Related to Fig. 5. Spearman correlation analysis of representative DEPs (A2M and BCHE) and lipids between four groups (Ctr, PCOS, Ob, or PC-Ob).

Acknowledgements
We thank the assistance of staff from Experimental Animal Center and Analysis & Testing Center of Nanjing Medical University and Anhui Medical University.

Authors' contributions
Qian Li, Dong Zhang, Ping Zhou, Xian-Zhe Gu, and Jie Chen designed the research. Mei-Ling Chen is charge of most of the experiments, data collection & analysis and figure preparation, wherein Shu-Ping Zhang, Jie Yang, Peng-Fei Qin, and Jia-Qi Liu made substantial contribution. Peng-Fei Qin is in the charge of patient plasma collection and information organization. All others assisted in some of the experiments. Qian Li wrote the manuscript with the assistance of Mei-Ling Chen, Shu-Ping Zhang, Jie Yang, Peng-Fei Qin, and Jia-Qi Liu; Dong Zhang, Ping Zhou, Xian-Zhe Gu, and Jie Chen proofread and gave advice. All authors read and approved the final manuscript.

Funding
The author(s) declare financial support was received for the research, authorship, and/or publication of this article. This work was financially supported by National Key R&D Program of China to Dong Zhang (Grant No: 2023YFA1800303), the General Program of the National Natural Science Foundation of China to Qian Li (Grant No: 81971353).

Data availability
The protocols and data that support the findings of this study are available from the corresponding author upon reasonable request. Plasma Metabolome data in supplementary datasets 2 have also been deposited into Zenodo, the DOI is https://doi.org/10.5281/zenodo.13833895. Raw exosome proteomics data corresponding to supplementary dataset 1 have been submitted to PRIDE (ProteomeXchange Consortium), the accession code was 1-20240821-111911-2362754.

Declarations

Ethics approval and consent to participate
All participants provided written informed consent for the use of their data for research purposes. The study protocol was approved by Human Medical Ethics Committee (HMEC) of Nanjing Women and Children's Healthcare Hospital (approval no. 2023KY-013).

Competing interests
The authors declare no competing interests.

Author details
[1]Department of Gynaecology and Obstetrics, NHC Key Laboratory of Study on Abnormal Gametes and Reproductive Tract of Anhui Medical University, the First Affiliated Hospital of Anhui Medical University, , 218 Jixi Road, No 81 Meishan Road, Hefei, Anhui 230022, China
[2]Department of Gynecology, Women's Hospital of Nanjing Medical University & Nanjing Women and Children's Healthscare Hospital, 123 Tianfei Lane, Mochou Road, Nanjing, Jiangsu 210018, China
[3]State Key Lab of Reproductive Medicine and Offspring Health, Nanjing Medical University, 101 Longmian Avenue, Nanjing, Jiangsu 211166, China
[4]Hefei Cancer Hospital, Chinese Academy of Sciences, 350 Shushanhu Road, Hefei, Anhui 230031, China
[5]Central Laboratory, the First Affiliated Hospital of Anhui Medical University, No 218 Jixi Road, Hefei, Anhui 230022, China

Received: 14 March 2025 / Accepted: 21 April 2026
Published online: 28 April 2026

References

1. Goodarzi MO, Dumesic DA, Chazenbalk G, Azziz R. Polycystic ovary syndrome: etiology, pathogenesis and diagnosis. Nat Rev Endocrinol. 2011;7(4):219–31.
2. Balen AH, Morley LC, Misso M, Franks S, Legro RS, Wijeyaratne CN, Stener-Victorin E, Fauser BC, Norman RJ, Teede H. The management of anovulatory infertility in women with polycystic ovary syndrome: an analysis of the evidence to support the development of global WHO guidance. Hum Reprod Update. 2016;22(6):687–708.
3. Han Q, Wang J, Li W, Chen ZJ, Du Y. Androgen-induced gut dysbiosis disrupts glucolipid metabolism and endocrinal functions in polycystic ovary syndrome. Microbiome. 2021;9(1):101.
4. Zhang KH, Zhang FF, Zhang ZL, Fang KF, Sun WX, Kong N, Wu M, Liu HO, Liu Y, Li Z, Cai QQ, Wang Y, Wei QW, Lin PC, Lin Y, Xu W, Xu CJ, Yuan YY, Zhao SM. Follicle stimulating hormone controls granulosa cell glutamine synthesis to regulate ovulation. Protein Cell. 2024;15(7):512–29.
5. Moran LJ, Misso ML, Wild RA, Norman RJ. Impaired glucose tolerance, type 2 diabetes and metabolic syndrome in polycystic ovary syndrome: a systematic review and meta-analysis. Hum Reprod Update. 2010;16(4):347–63.
6. Torstensson S, Ascani A, Risal S, Lu H, Zhao A, Espinosa A, Lindgren E, Johansson MH, Eriksson G, Barakat M, Karlsson MCI, Svensson C, Benrick A, Stener-Victorin E. Androgens modulate the immune profile in a mouse model of polycystic ovary syndrome. Adv Sci (Weinh). 2024;20:e2401772.
7. Wang J, Yin T, Liu S. Dysregulation of immune response in PCOS organ system. Front Immunol. 2023;14:1169232.
8. Salehi R, Asare-Werehene M, Wyse BA, Abedini A, Pan B, Gutsol A, Jahangiri S, Szaraz P, Burns KD, Vanderhyden B, Li J, Burger D, Librach CL, Tsang BK. Granulosa cell-derived miR-379-5p regulates macrophage polarization in polycystic ovarian syndrome. Front Immunol. 2023;14:1104550.
9. Liu Y, Liu H, Li Z, Fan H, Yan X, Liu X, Xuan J, Feng D, Wei X. The release of peripheral immune inflammatory cytokines promote an inflammatory cascade in PCOS patients via altering the follicular microenvironment. Front Immunol. 2021;12:685724.
10. Qi X, Yun C, Sun L, Xia J, Wu Q, Wang Y, Wang L, Zhang Y, Liang X, Wang L, Gonzalez FJ, Patterson AD, Liu H, Mu L, Zhou Z, Zhao Y, Li R, Liu P, Zhong C, Pang Y, Jiang C, Qiao J. Gut microbiota-bile acid-interleukin-22 axis orchestrates polycystic ovary syndrome. Nat Med. 2019;25(8):1225–33.
11. Stokkeland LMT, Giskeødegård GF, Ryssdal M, Jarmund AH, Steinkjer B, Madssen TS, Stafne SN, Stridsklev S, Løvvik TS, Iversen AC, Vanky E. Changes in serum cytokines throughout pregnancy in women with polycystic ovary syndrome. J Clin Endocrinol Metab. 2022;107(1):39–52.
12. Gao L, Zhao Y, Wu H, Lin X, Guo F, Li J, Long Y, Zhou B, She J, Zhang C, Sheng J, Jin L, Wu Y, Huang H. Polycystic ovary syndrome fuels cardiovascular inflammation and aggravates ischemic cardiac injury. Circulation. 2023;148(24):1958–73.
13. Hu M, Zhang Y, Li X, Cui P, Sferruzzi-Perri AN, Brännström M, Shao LR, Billig H. TLR4-Associated IRF-7 and NFκB signaling act as a molecular link between androgen and metformin activities and cytokine synthesis in the PCOS endometrium. J Clin Endocrinol Metab. 2021;106(4):1022–40.
14. Deng M, Li Z, Chen S, Wang H, Sun L, Tang J, Luo L, Zhang X, Xu H, Dai Z. Exploring the heterogeneity of hepatic and pancreatic fat deposition in obesity: implications for metabolic health. Front Endocrinol (Lausanne). 2024;15:1447750.
15. Zhou Y, Xie Y, Dong J, He K. Associations between metabolic overweight/obesity phenotypes and mortality risk among patients with chronic heart failure. Front Endocrinol (Lausanne). 2024;15:1445395.
16. Mao L, Lu J, Hou Y, Nie T. Directly targeting PRDM16 in thermogenic adipose tissue to treat obesity and its related metabolic diseases. Front Endocrinol (Lausanne). 2024;15:1458848.
17. Kositanurit W, Siritaweechai N, Varachotisate P, Burana C, Sukswai N, Surintrspanont J, Siriviriyakul P, Kaikaew K, Werawatganon D. Genistein mitigates diet-induced obesity and metabolic dysfunctions in gonadectomized mice with some sex-differential effects. Front Endocrinol (Lausanne). 2024;15:1392866.
18. Ying W, Fu W, Lee YS, Olefsky JM. The role of macrophages in obesity-associated islet inflammation and β-cell abnormalities. Nat Rev Endocrinol. 2020;16(2):81–90.
19. Gomes AC, Hoffmann C, Mota JF. The human gut microbiota: Metabolism and perspective in obesity. Gut Microbes. 2018;9(4):308–25.
20. Darbre PD. Endocrine disruptors and obesity. Curr Obes Rep. 2017;6(1):18–27.
21. Azzu V, Vacca M, Virtue S, Allison M, Vidal-Puig A. Adipose tissue-liver cross talk in the control of whole-body metabolism: implications in nonalcoholic fatty liver disease. Gastroenterology. 2020;158(7):1899–912.

22. Lopez-Jimenez F, Almahmeed W, Bays H, Cuevas A, Di Angelantonio E, le Roux CW, Sattar N, Sun MC, Wittert G, Pinto FJ, Wilding JPH. Obesity and cardiovascular disease: mechanistic insights and management strategies. Eur J Prev Cardiol. 2022;29(17):2218–37. A joint position paper by the World Heart Federation and World Obesity Federation.
23. Gregor MF, Hotamisligil GS. Inflammatory mechanisms in obesity. Annu Rev Immunol. 2011;29:415–45.
24. Park J, Morley TS, Kim M, Clegg DJ, Scherer PE. Obesity and cancer–mechanisms underlying tumour progression and recurrence. Nat Rev Endocrinol. 2014;10(8):455–65.
25. Eng PC, Phylactou M, Qayum A, Woods C, Lee H, Aziz S, Moore B, Miras AD, Comninos AN, Tan T, Franks S, Dhillo WS, Abbara A. Obesity-related hypogonadism in women. Endocr Rev. 2024;45(2):171–89.
26. Haase CL, Varbo A, Laursen PN, Schnecke V, Balen AH. Association between body mass index, weight loss and the chance of pregnancy in women with polycystic ovary syndrome and overweight or obesity: a retrospective cohort study in the UK. Hum Reprod. 2023;38(3):471–81.
27. de Zegher F, Lopez-Bermejo A, Ibáñez L. Adipose tissue expandability and the early origins of PCOS. Trends Endocrinol Metab. 2009;20(9):418–23.
28. Legro RS. Obesity and PCOS: implications for diagnosis and treatment. Semin Reprod Med. 2012;30(6):496–506.
29. Vulcan T, Suciu TS, Lenghel LM, Toma VA, Decea N, Moldovan R, Mitrea DR, Baldea I, Filip GA. The impact of vitamin D3 administration and of high fat diet on oxidative stress and inflammation in experimentally induced polycystic ovary syndrome. Med Pharm Rep. 2024;97(4):516–27.
30. Ressler IB, Grayson BE, Ulrich-Lai YM, Seeley RJ. Diet-induced obesity exacerbates metabolic and behavioral effects of polycystic ovary syndrome in a rodent model. Am J Physiol Endocrinol Metab. 2015;308(12):E1076–84.
31. Wu RX, Dong YY, Yang PW, Wang L, Deng YH, Zhang HW, Huang XY. CD36- and obesity-associated granulosa cells dysfunction. Reprod Fertil Dev. 2019;31(5):993–1001.
32. Oyama K, Raz I, Cahn A, Kuder J, Murphy SA, Bhatt DL, Leiter LA, McGuire DK, Wilding JPH, Park KS, Goudev A, Diaz R, Špinar J, Gause-Nilsson IAM, Mosenzon O, Sabatine MS, Wiviott SD. Obesity and effects of dapagliflozin on cardiovascular and renal outcomes in patients with type 2 diabetes mellitus in the DECLARE-TIMI 58 trial. Eur Heart J. 2022;43(31):2958–67.
33. Teede HJ, Tay CT, Laven J, Dokras A, Moran LJ, Piltonen TT, Costello MF, Boivin J, M Redman L, A Boyle J, Norman RJ, Mousa A, Joham AE. International PCOS Network. Recommendations from the 2023 International evidence-based guideline for the assessment and management of polycystic ovary syndrome. Fertil Steril. 2023;120(4):767-793.
34. Jiang X, Li J, Zhang B, Hu J, Ma J, Cui L, Chen ZJ. Differential expression profile of plasma exosomal microRNAs in women with polycystic ovary syndrome. Fertil Steril. 2021;115(3):782–92.
35. Idicula-Thomas S, Gawde U, Bhaye S, Pokar K, Bader GD. Meta-analysis of gene expression profiles of lean and obese PCOS to identify differentially regulated pathways and risk of comorbidities. Comput Struct Biotechnol J. 2020;18:1735–45.
36. Sun C, Cao C, Zhao T, Guo H, Fleming BC, Owens B, Beveridge J, McAllister S, Wei L. A2M inhibits inflammatory mediators of chondrocytes by blocking IL-1β/NF-κB pathway. J Orthop Res. 2023;41(1):241–8.
37. Jiang D, Shao Y, Zhang S, Li C. A2M possesses anti-bacterial functions by recruiting and enhancing phagocytosis through GRP78 in an echinoderm. Int J Biol Macromol. 2024;265(Pt 2):131016.
38. Federici Canova D, Pavlov AM, Norling LV, Gobbetti T, Brunelleschi S, Le Fauder P, Cenac N, Sukhorukov GB, Perretti M. Alpha-2-macroglobulin loaded microcapsules enhance human leukocyte functions and innate immune response. J Control Release. 2015;217:284–92.
39. Liu S, Ge J, Chu Y, Cai S, Wu J, Gong A, Zhang J. Identification of hub cuproptosis related genes and immune cell infiltration characteristics in periodontitis. Front Immunol. 2023;14:1164667.
40. Uddin MN, Yao Y, Mondal T, Matala R, Manley K, Lin Q, Lawrence DA. Immunity and autoantibodies of a mouse strain with autistic-like behavior. Brain Behav Immun Health. 2020;4:100069.
41. Zhou Y, Li X, Ng L, Zhao Q, Guo W, Hu J, Zhong J, Su W, Liu C, Su S. Identification of copper death-associated molecular clusters and immunological profiles in rheumatoid arthritis. Front Immunol. 2023;14:1103509.
42. Li Y, Wu S, Zhao Y, Dinh T, Jiang D, Selfridge JE, Myers G, Wang Y, Zhao X, Tomchuck S, Dubyak G, Lee RT, Estfan B, Shapiro M, Kamath S, Mohamed A, Huang SC, Huang AY, Conlon R, Krishnamurthi S, Eads J, Willis JE, Khorana AA, Bajor D, Wang Z. Neutrophil extracellular traps induced by chemotherapy inhibit tumor growth in murine models of colorectal cancer. J Clin Invest. 2024;134(5):e175031.
43. Cheng N, Liang Y, Du X, Ye RD. Serum amyloid a promotes LPS clearance and suppresses LPS-induced inflammation and tissue injury. EMBO Rep. 2018;19(10):e45517.
44. Chen VP, Gao Y, Geng L, Stout MB, Jensen MD, Brimijoin S. Butyrylcholinesterase deficiency promotes adipose tissue growth and hepatic lipid accumulation in male mice on high-fat diet. Endocrinology. 2016;157(8):3086–95.
45. McGehee DS, Krasowski MD, Fung DL, Wilson B, Gronert GA, Moss J. Cholinesterase inhibition by potato glycoalkaloids slows mivacurium metabolism. Anesthesiology. 2000;93(2):510–9.
46. Alzahrani F, Kuwahara H, Long Y, Al-Owain M, Tohary M, AlSayed M, Mahnashi M, Fathi L, Alnemer M, Al-Hamed MH, Lemire G, Boycott KM, Hashem M, Han W, Al-Maawali A, Al Mahrizi F, Al-Thihli K, Gao X, Alkuraya FS. Recessive, deleterious variants in SMG8 expand the role of nonsense-mediated decay in developmental disorders in humans. Am J Hum Genet. 2020;107(6):1178–85.
47. Usuki F, Yamashita A, Shiraishi T, Shiga A, Onodera O, Higuchi I, Ohno S. Inhibition of SMG-8, a subunit of SMG-1 kinase, ameliorates nonsense-mediated mRNA decay-exacerbated mutant phenotypes without cytotoxicity. Proc Natl Acad Sci U S A. 2013;110(37):15037–42.
48. Edwards PD, Boonstra R. Glucocorticoids and CBG during pregnancy in mammals: diversity, pattern, and function. Gen Comp Endocrinol. 2018;259:122–30.
49. Pei Y, Lv S, Shi Y, Jia J, Ma M, Han H, Zhang R, Tan J, Zhang X. RAB21 controls autophagy and cellular energy homeostasis by regulating retromer-mediated recycling of SLC2A1/GLUT1. Autophagy. 2023;19(4):1070–86.

Publisher's note